ACADEMIC PRESS

Available online at www.sciencedirect.com

SCIENCE DIRECT®

Journal of Sound and Vibration 264 (2003) 91–116

JOURNAL OF SOUND AND VIBRATION

www.elsevier.com/locate/jsvi

Lateral moment and axial force excitation of deep beams; point and point-cross mobilities

B.A.T. Petersson*

Institute of Technical Acoustics, Technical University of Berlin, Einsteinufer 25, 10587 Berlin, Germany

Received 25 February 2002; accepted 27 May 2002

Abstract

The cross-coupling at an excited interface between, on the one hand, a lateral moment and an axial translational velocity and, on the other, an axial force and a lateral rotational velocity is studied for an arbitrarily deep beam. Complete descriptions are developed for the two associated point-cross mobility elements. In addition, the point mobility is established relating to an axial force excitation at an edge of the beam. From the theoretical results it can be concluded that reciprocity with respect to the point-cross mobility elements is strictly, only valid in the hypothetical case of point excitation. The numerical results demonstrate, however, that reciprocity can be invoked in an approximate sense also for realistic excitation conditions. Moreover, it is shown that a reduction of an axial force excitation, remote from the neutral layer, to a combined force and moment excitation at the neutral layer is not applicable except for very small Helmholtz numbers. Finally, it can be concluded that the shear-tensional nearfield affects the point-cross mobilities in the case of two-dimensional beam-like structures. A similar influence is established for the axial point force mobility but an unambiguous description has not been found.

1. Introduction

In many engineering applications involving vibrating machinery, deep beams are favoured installation positions, the argument being that high support stiffness is realized. In a previous study [1], three primary aspects of nearfield effects in such deep beams as well as thick plates were treated. First, can a refined, approximate theory such as Mindlin [2] or Timoshenko [3] theory for plate- and beam-like structures, respectively, approximately describe the shear-tensional nearfield effects? Second, are the nearfield effects critically dependent on the actual excitation conditions

*Tel.: +49-30-314-22931; fax: +49-30-314-25135.
E-mail address: b.a.t.petersson@tu-berlin.de (B.A.T. Petersson).

0022-460X/03/$ - see front matter
doi:10.1016/S0022-460X(02)01167-7

such as the stress at the excitation area and third, can the local deformation be satisfactorily approximated in closed form? With respect to the first aspect it was concluded that cross-sectionally integrated theories are incapable of capturing the shear-tensional nearfield effects and hence are inapplicable, whenever a contact area is comparable in dimensions to the depths or thicknesses of involved structures. Regarding the second aspect, it was demonstrated that the local deformation is only weakly dependent on the excitation conditions and primarily influenced by the size of the contact area. Finally, it was possible to develop valid, closed-form approximations for both force and moment excitation of plates whereas corresponding relations in the case of deep beams are confined to moment excitation. Subsequently, the deep beam was further examined [4] and closed-form approximations for the point force mobility were established.

Although deep beam and thick plates have received some attention, see e.g., Refs. [5–9], it is almost exclusively the direct frequency response at the 'point' of excitation that has been addressed. For source–receiver systems involving multiple components of excitation; however, the transmission of vibrational power also depends on the amount of cross-coupling. Herein, the structure-borne sound transmission to beam-like supports is revisited. Partly prompted by preliminary results indicating non-reciprocal point-cross mobilities for, on the one hand, axial force to rotational velocity and lateral moment to axial velocity on the other, these elements are addressed. Moreover, the axial point force mobility is also included. In this context also, three questions are posed. Can reciprocity be demonstrated for the point-cross mobilities, can cross-sectionally integrated beam theories be employed in predictions and what is the influence of shear-tensional nearfields?

2. Theoretical analysis

2.1. Lateral moment excitation to translational and lateral, rotational responses

Consider the beam of rectangular cross-section and total depth H, depicted in Fig. 1, subject to a moment excitation via a soft or rigid indenter at the upper edge such that the stress is uniform across the beam width.

For this case the translatory velocities, at the excited edge, $y = h = H/2$, are given by [1,5]

$$v_x = -\frac{\omega}{4\pi G}\int_{-\infty}^{\infty} k\hat{\sigma}(k)\left(\frac{(2k^2-k_T^2)\tan(q_L h)+2q_L q_T\tan(q_T h)}{N_1} + \frac{(2k^2-k_T^2)\cot(q_L h)+2q_L q_T\cot(q_T h)}{N_2}\right)e^{ikx}\,dk \tag{1}$$

and

$$v_y = -\frac{i\omega}{4\pi G}k_T^2\int_{-\infty}^{\infty} q_L\hat{\sigma}(k)\left(\frac{1}{N_1}-\frac{1}{N_2}\right)e^{ikx}\,dk, \tag{2}$$

where

$$N_1 = (2k^2-k_T^2)\tan(q_L h)+4k^2 q_L q_T\tan(q_T h), \tag{3a}$$

$$N_2 = (2k^2-k_T^2)\cot(q_L h)+4k^2 q_L q_T\cot(q_T h) \tag{3b}$$

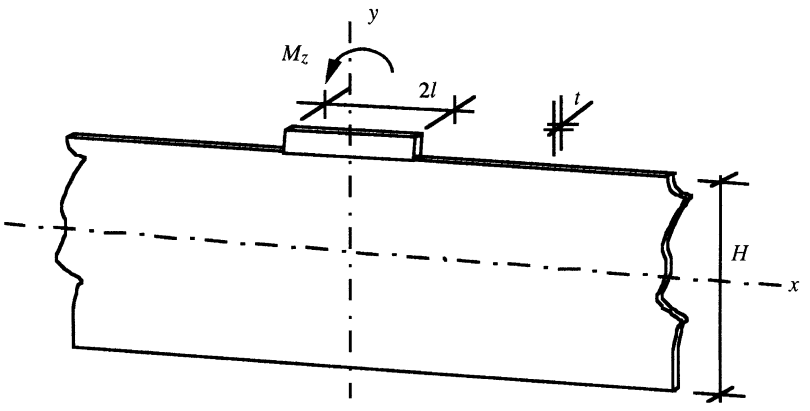

Fig. 1. Moment excited deep beam.

with

$$q_{L,T} = \begin{cases} -\sqrt{k_{L,T}^2 - k^2}, & k^2 \leqslant k_{L,T}^2, \\ \mathrm{i}\sqrt{k^2 - k_{L,T}^2}, & k_{L,T}^2 < k^2. \end{cases} \tag{4}$$

All symbols are defined in Appendix B.

The excitation wavenumber spectra for soft and rigid indenters, derived in Ref. [1], are given by

$$\hat{\sigma}_s(k) = -\frac{3\mathrm{i}M_z}{tl}\frac{1}{kl}\left[\frac{\sin kl}{kl} - \cos kl\right] \tag{5a}$$

and

$$\hat{\sigma}_r(k) = -\frac{2\mathrm{i}M_z}{tl}\mathrm{J}_1(kl). \tag{5b}$$

For the point mobility, the extension to a contact area that is large in comparison with the governing wavelength is defined on a complex power basis [10], i.e.,

$$Y_{wM}^{\infty} = \int_S v\sigma^* \,\mathrm{d}S \Big/ \left|\int_S \sigma x \,\mathrm{d}S\right|^2.$$

With this definition, the point mobility from a lateral moment M_z to a lateral rotational velocity w_z was derived as [1]

$$Y_{wM}^{\infty} = \frac{\mathrm{i}\omega}{2\pi G t l^2} k_T^2 \int_0^{\infty} q_L E(k)\left(\frac{1}{N_1} - \frac{1}{N_2}\right)\mathrm{d}k \tag{6}$$

with the excitation wavenumber spectra

$$E(k) = \begin{cases} \left(\dfrac{3}{kl}\right)^2\left(\dfrac{\sin kl}{kl} - \cos kl\right)^2, & \text{soft indenter}, \\ (2\mathrm{J}_1(kl))^2, & \text{rigid indenter}. \end{cases}$$

Regarding the cross mobilities, a power-based averaging is not appropriate since the excitation and response components are orthogonal. Instead, a spatial average is introduced so that

$$Y_{vM}^{\infty} = \frac{1}{2l}\int_{2l} v(x)\,\mathrm{d}x \Big/ \left|\int_{2l} \sigma t x\,\mathrm{d}x\right|. \tag{7}$$

The cross mobility from moment excitation to longitudinal response is thence derived to be

$$Y_{v_x M_z}^{\infty} = \frac{\mathrm{i}\omega}{4\pi G t l}\int_{-\infty}^{\infty} k\bar{E}(k)\left(\frac{(2k^2-k_T^2)\tan(q_L h)+2q_L q_T\tan(q_T h)}{N_1} + \frac{(2k^2-k_T^2)\cot(q_L h)+2q_L q_T\cot(q_T h)}{N_2}\right)\mathrm{d}k. \tag{8}$$

Analogously, the cross mobility from moment excitation to transverse response can be derived and is given by

$$Y_{v_y M_z}^{\infty} = -\frac{\mathrm{i}\omega k_T^2}{4\pi G t l}\int_{-\infty}^{\infty} q_L\bar{E}(k)\left(\frac{1}{N_1}+\frac{1}{N_2}\right)\mathrm{d}k. \tag{9}$$

In Eqs. (8) and (9),

$$\bar{E}(k) = \begin{cases} \dfrac{3}{kl}\left[\dfrac{\sin kl}{kl}-\cos kl\right]\dfrac{\sin kl}{kl}, & \text{soft indenter,} \\ 2\mathrm{J}_1(kl)\dfrac{\sin kl}{kl}, & \text{rigid indenter.} \end{cases}$$

Since the integrand in Eq. (9) is an odd function then, irrespective of type of indenter, this point-cross mobility vanishes identically.

In the case that the beam is very deep, the tangents and cotangents of the denominators N_1 and N_2 tend to i and $-$i, respectively which means that

$$Y_{v_x M_z}^{\infty} \to -\frac{\mathrm{i}\omega}{4\pi G t l}\int_{-\infty}^{\infty} k\bar{E}(k)\left(\frac{1}{N}\right)[2(2k^2-k_T^2)+4q_L q_T]\,\mathrm{d}k \tag{8a}$$

with

$$N = (2k^2-k_T^2)+4q_L q_T. \tag{3c}$$

Due to the behaviour of the integrand for both kinds of indenters, however, a limiting value process for low frequencies, similar to that employed in Ref. [1] for the moment mobility, is not applicable. One can thus expect a qualitatively complicated dependence of the local deformation on the beam height as well as length of the indenter, resembling that found for the transverse point force mobility.

2.2. Axial force excitation to translational and lateral, rotational responses

In this case, the beam is subject to a force excitation in the axial direction via the soft or rigid indenter at the upper edge as depicted in Fig. 2. It is assumed that the force is uniformly distributed across the width of the beam.

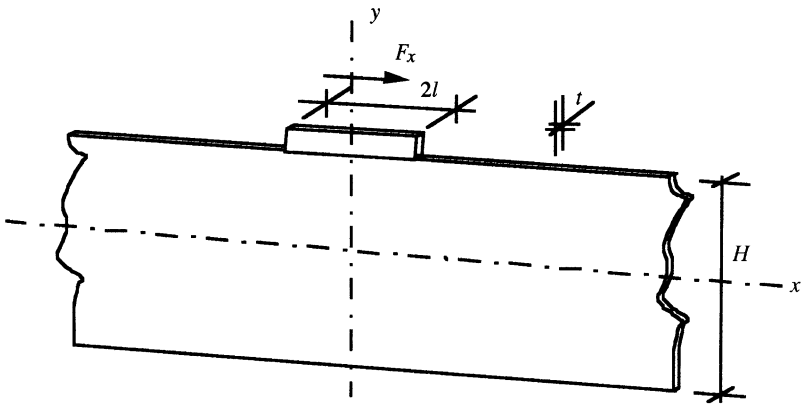

Fig. 2. Axially force excited deep beam.

From the equation of motion and the constitutive equations, with the changes of the boundary conditions for the present case observed,

$$\tau_{yx}(x,h)=\frac{F_x}{2lt},\quad \tau_{yx}(x,-h)=\sigma_y(x,h)=\sigma_y(x,-h)=0$$

one finds that the set of equations to be solved can be written as

$$\frac{\mathrm{i}\omega}{2G}\boldsymbol{\sigma}=\mathbf{C}\boldsymbol{\Phi}, \tag{10}$$

where

$$\boldsymbol{\sigma}=\begin{Bmatrix}\sigma(x,h)\\ \sigma(x,-h)\\ \tau(x,h)\\ \tau(x,-h)\end{Bmatrix}=\begin{Bmatrix}0\\0\\ \hat{\tau}\\0\end{Bmatrix}\mathrm{e}^{\mathrm{i}kx} \tag{11a, b}$$

are the boundary conditions imposed and

$$\boldsymbol{\Phi}=\begin{Bmatrix}\Phi_1\\ \Phi_2\\ \Psi_1\\ \Psi_2\end{Bmatrix} \tag{12}$$

are the unknown coefficients of the potentials of the assumed solution. Solving for the coefficients, see Appendix A, the potentials are found to be given by

$$\Phi=\left\{\frac{-(1-v)\mathrm{i}kq_Tc_T\cos(q_Ly)}{d_1}+\frac{(1-v)\mathrm{i}kq_Ts_T\sin(q_Ly)}{d_2}\right\}\mathrm{e}^{\mathrm{i}kx} \tag{13a}$$

and

$$\Psi=\left\{\frac{(q_L^2+vk^2)s_L\cos(q_Ty)}{d_2}+\frac{(q_L^2+vk^2)c_L\sin(q_Ty)}{d_1}\right\}\mathrm{e}^{\mathrm{i}kx}, \tag{13b}$$

where

$$d_1 = (q_L^2 + vk^2)(k^2 - q_T^2)c_L s_T - 2(1-v)k^2 q_T q_L c_T s_L \tag{14a}$$

and

$$d_2 = (q_L^2 + vk^2)(k^2 - q_T^2)c_T s_L - 2(1-v)k^2 q_T q_L c_L s_T. \tag{14b}$$

From Eq. (A.3), the spectral components of the velocities for the present case can be derived as

$$v_x = \frac{\mathrm{i}\omega}{2G} qT \left\{ \frac{2k^2 \dfrac{\sin(q_L y)}{\sin(q_L h)} - (2k^2 - k_T^2)\dfrac{\sin(q_T y)}{\sin(q_T h)}}{(2k^2 - k_T^2)^2 \cot(q_T h) + 4k^2 q_T q_L \cot(q_L h)} \right.$$
$$\left. - \frac{2k^2 \dfrac{\cos(q_L y)}{\cos(q_L h)} - (2k^2 - k_T^2)\dfrac{\cos(q_T y)}{\cos(q_T h)}}{(2k^2 - k_T^2)^2 \tan(q_T h) + 4k^2 q_T q_L \tan(q_L h)} \right\} \mathrm{e}^{\mathrm{i}kx}$$

and

$$v_y = \frac{\omega k}{2G} \left\{ \frac{(2k^2 - k_T^2)\dfrac{\sin(q_T y)}{\cos(q_T h)} + 2q_L q_T \dfrac{\sin(q_L y)}{\cos(q_L h)}}{(2k^2 - k_T^2)^2 \tan(q_T h) + 4k^2 q_L q_T \tan(q_L h)} \right.$$
$$\left. + \frac{(2k^2 - k_T^2)\dfrac{\cos(q_T y)}{\sin(q_T h)} + 2q_L q_T \dfrac{\cos(q_L y)}{\sin(q_L h)}}{(2k^2 - k_T^2)^2 \cot(q_T h) + 4k^2 q_L q_T \cot(q_L h)} \right\} \mathrm{e}^{\mathrm{i}kx}.$$

The excitation wavenumber spectra for soft and rigid indenters, can be derived to be,

$$\hat{\tau}_s(k) = \frac{F_x}{t} \frac{\sin kl}{kl} \tag{15a}$$

and

$$\hat{\tau}_r(k) = \frac{F_x}{t} \mathrm{J}_0(kl). \tag{15b}$$

For the point mobility, the extension to a contact area, which is large in comparison with the governing wavelength, is again obtained via the complex power [10], i.e.,

$$Y^{\infty}_{v_x F_x} = \int_S v\tau^* \,\mathrm{d}S \Big/ \left| \int_S \tau \,\mathrm{d}S \right|^2.$$

This means that after some minor manipulations, the point mobility from an axial to an axial translational velocity is found to be given by

$$Y^{\infty}_{v_x F_x} = \frac{\mathrm{i}\omega}{2\pi G t} k_T^2 \int_0^{\infty} q_T E(k) \left(\frac{\tan(q_L h)\tan(q_T h)}{N_1} - \frac{\cot(q_L h)\cot(q_T h)}{N_2} \right) \mathrm{d}k \tag{16}$$

with

$$E(k) = \begin{cases} \left(\dfrac{\sin kl}{kl}\right)^2, & \text{soft indenter,} \\ (\mathrm{J}_0(kl))^2, & \text{rigid indenter} \end{cases} \tag{17}$$

and N_1 as well as N_2 retained from the previous section.

Regarding the cross mobilities, the spatial average is employed which leads to

$$Y^{\infty}_{v_y F_x} = \frac{1}{2l}\int_{2l} v(x)\,\mathrm{d}x \Big/ \int_{2l} \tau t\,\mathrm{d}x$$

and

$$Y^{\infty}_{v_z F_x} = \frac{1}{2l}\int_{2l} \frac{\partial}{\partial x}(v_y(x))\,\mathrm{d}x \Big/ \int_{2l} \tau t\,\mathrm{d}x,$$

respectively.

Thus,

$$Y^{\infty}_{v_y F_x} = \frac{\omega}{4\pi G t}\int_{-\infty}^{\infty} k\bar{E}(k)\left(\frac{(2k^2 - k_T^2)\tan(q_L h) + 2q_L q_T \tan(q_T h)}{N_1} + \frac{(2k^2 - k_T^2)\cot(q_L h) + 2q_L q_T \cot(q_T h)}{N_2}\right)\mathrm{d}k, \tag{18}$$

which, in view of the integrand, vanishes identically whereas

$$Y^{\infty}_{w_y F_x} = \frac{\mathrm{i}\omega}{2\pi G t}\int_{-\infty}^{\infty} k^2\bar{E}(k)\left(\frac{(2k^2 - k_T^2)\tan(q_L h) + 2q_L q_T \tan(q_T h)}{N_1} + \frac{(2k^2 - k_T^2)\cot(q_L h) + 2q_L q_T \cot(q_T h)}{N_2}\right)\mathrm{d}k \tag{19}$$

does not. The excitation wavenumber spectra

$$\bar{E}(k) = \begin{cases} \left[\dfrac{\sin kl}{kl}\right]^2, & \text{soft indenter,} \\ \mathrm{J}_0(kl)\dfrac{\sin kl}{kl}, & \text{rigid indenter} \end{cases} \tag{20}$$

are valid for both Eqs. (18) and (19).

Upon comparing the cross mobilities in Eqs. (8) and (19), it is evident that these differ. Accordingly, one can conclude that the point-cross mobilities from force to rotational velocity and moment to axial velocity strictly constitute a reciprocal pair only in the hypothetical case of a point excitation in which case, the mobility becomes

$$Y^{\infty}_{v_x M_z} = Y^{\infty}_{w_z F_x} = \frac{\mathrm{i}\omega}{2\pi G t}\int_0^{\infty} k^2\left(\frac{(2k^2 - k_T^2)\tan(q_L h) + 2q_L q_T \tan(q_T h)}{N_1} + \frac{(2k^2 - k_T^2)\cot(q_L h) + 2q_L q_T \cot(q_T h)}{N_2}\right)\mathrm{d}k.$$

In the case that the beam is very deep, the tangents tend to i and cotangents to $-$i as before which, in this case, means that

$$Y^{\infty}_{w_z F_x} \to -\mathrm{i}\,\frac{\omega}{\pi G t}\,\frac{2k_T^2}{(1-v)}\int_0^{\infty}\frac{q_L E(k)}{N}\,\mathrm{d}k, \tag{16a}$$

whereas

$$Y^{\infty}_{w_z F_x} \to \frac{\mathrm{i}\omega}{\pi G t}\int_0^{\infty} k^2 \bar{E}(k)\left(\frac{(2k^2-k_T^2)+2q_L q_T}{N}\right)\mathrm{d}k \tag{19a}$$

with N retained from the previous section.

For both kinds of indenters, the behaviour of the integrand in Eq. (16a) effectively prevents a limiting value process for low frequencies. Hence, a qualitatively complicated influence of the beam height and indenter length can be expected.

Regarding the cross mobility from a force to the rotational velocity, one finds in the limit of infinite beam depth that for a soft indenter,

$$Y^{\infty}_{w_z F_x} \to -\frac{\mathrm{i}\omega}{4Gtl}\,\frac{(1-v)}{(1+v)} \approx -\frac{\mathrm{i}\omega}{8Gtl}. \tag{21}$$

This means that the shear-tensional nearfield yields a response of a 'negative spring', which is controlled by the elasticity in shear. A corresponding estimate of the local deformation in the case of a rigid indenter has not been found. One may, however, cautiously infer a similar dependence as for the soft indenter from the similarity of the excitation wavenumber spectra for small Helmholtz numbers. This is furthermore supported by a comparison of the contributions from the shear-tensional near field to the point moment mobility for different indenters [1] where the variations were demonstrated small.

3. Numerical analysis

3.1. Lateral moment excitation

The point and cross mobilities derived in a previous section can be analyzed numerically. For the numerical analysis it is convenient to use normalized versions. As employed in Ref. [1], the point moment mobility is normalized with respect to half the magnitude of the corresponding mobility for slender beams, which yields

$$\begin{aligned}\overline{Y^{\infty}_{wM}} &= \frac{Y^{\infty}_{wM}}{(\omega/4Bk_B)}\\ &= -\mathrm{i}\,\frac{2}{\pi}\left(\frac{(1+\nu)}{6}\right)^{3/4}\left(\frac{H}{l}\right)^2\sqrt{k_T H}\int_0^{\infty}\sqrt{\frac{(1-\nu)}{2}-\kappa^2}\,E_M(\kappa)\left(\frac{1}{\overline{N_1}}-\frac{1}{\overline{N_2}}\right)\mathrm{d}\kappa,\end{aligned} \tag{22}$$

where

$$E_M(\kappa) = \begin{cases} \left(\dfrac{3}{\kappa k_T l}\right)^2 \left(\dfrac{\sin \kappa k_T l}{\kappa k_T l} - \cos \kappa k_T l\right)^2, & \text{soft indenter,} \\ (2\mathrm{J}_1(\kappa k_T l))^2, & \text{rigid indenter} \end{cases} \tag{23}$$

and

$$\overline{N_1} = (2\kappa^2 - 1)^2 \tan\left(k_T h \sqrt{\frac{(1-v)}{2} - \kappa^2}\right) + 4\kappa^2 \sqrt{\frac{(1-v)}{2} - \kappa^2}\sqrt{1-\kappa^2}\,\tan(k_T h\sqrt{1-\kappa^2}), \tag{24a}$$

$$\overline{N_2} = (2\kappa^2 - 1)^2 \cot\left(k_T h \sqrt{\frac{(1-v)}{2} - \kappa^2}\right) + 4\kappa^2 \sqrt{\frac{(1-v)}{2} - \kappa^2}\sqrt{1-\kappa^2}\,\cot(k_T h\sqrt{1-\kappa^2}). \tag{24b}$$

Herein, the constitutive relation

$$\frac{k_L^2}{k_T^2} = \frac{(1-v)}{2} \tag{25}$$

is invoked.

In a similar manner, the point-cross mobility from a lateral moment to an axial translational velocity, normalized with respect to half the magnitude of the moment mobility of an Euler beam, multiplied by half its depth, take the form

$$\overline{Y^{\infty}_{v_x M_z}} = \frac{Y^{\infty}_{v_x M_z}}{(\omega H/8Bk_B)} = \frac{4\mathrm{i}}{\pi}\left(\frac{(1+v)}{6}\right)^{3/4}\left(\frac{H}{l}\right)^{3/2}\sqrt{k_T l} \times \int_{-\infty}^{\infty} \kappa \bar{E}_M(\kappa)\left(\frac{(2\kappa^2-1)\tan(k_T h\sqrt{\frac{(1-v)}{2}-\kappa^2}) + 2\sqrt{\frac{(1-v)}{2}-\kappa^2}\sqrt{1-\kappa^2}\,\tan(k_T h\sqrt{1-\kappa^2})}{\overline{N_1}} + \frac{(2\kappa^2-1)\cot(k_T h\sqrt{\frac{(1-v)}{2}-\kappa^2}) + 2\sqrt{\frac{(1-v)}{2}-\kappa^2}\sqrt{1-\kappa^2}\,\cot(k_T h\sqrt{1-\kappa^2})}{\overline{N_2}}\right)\mathrm{d}\kappa \tag{26}$$

with

$$\bar{E}_M(\kappa) = \begin{cases} \dfrac{3}{\kappa k_T l}\left[\dfrac{\sin \kappa k_T l}{\kappa k_T l} - \cos \kappa k_T l\right]\dfrac{\sin \kappa k_T l}{\kappa k_T l}, & \text{soft indenter,} \\ 2\mathrm{J}_1(\kappa k_T l)\dfrac{\sin \kappa k_T l}{\kappa k_T l}, & \text{rigid indenter.} \end{cases} \tag{27}$$

This normalization is introduced since for a rigid beam lamina, the moment is a free vector and can be seen acting at the neutral layer whereas the axial translational velocity at the edge is 'geometrically' enlarged.

Due to the branch points, the integrals have to be split in three main parts, cf. Ref. [1], whereby

$$\mathrm{I}I_{pq} \leftrightarrow \int_0^{\sqrt{(1-\nu)/2}}, \qquad \mathrm{II}\, I_{pq} \leftrightarrow \int_{\sqrt{(1-\nu)/2}}^{1} \quad \text{and} \quad \mathrm{III}I_{pq} \leftrightarrow \int_1^{\infty}.$$

The numerical procedure employed herein is similar to that described in Ref. [1] where the point moment mobility was treated.

For the third region it is necessary to carry out the integration in two steps of which the first addresses the actual integral and the second, the tail-integral, which must be computed asymptotically. In accordance with Ref. [1], one may set $\tanh(z)$ equal to unity for arguments larger than six. It must be observed, however, that in the present case, the argument is complex and a product of the two factors κ and $k_T h$ where the latter typically ranges from 0.01 to 100. This means that for $\kappa \geqslant 10$ and simultaneously $k_T l \geqslant 6$, the approximation

$$\mathrm{III}\, {}_{tail}I_{v_x M_z} = -2\left(\frac{1-\nu}{1+\nu}\right)\int_M^{\infty} \frac{\bar{E}_M(\kappa)}{\kappa}\,\mathrm{d}\kappa \tag{28}$$

is applicable considering the fact that $\kappa^2 \gg 1$. In view of the two conditions given above, the lower integration limit M is set to be

$$M \geqslant \mathrm{Max}\left[\sqrt{1 + (l/H)^2(12/k_T l)^2}, 10\right]. \tag{29}$$

Initially, far-reaching analyses were undertaken to ascertain physicality and computational stability of the numerical results. Hereby, the complete solution was split into its symmetric and antisymmetric parts for which pure asymptotic modes for small Helmholtz numbers are available, see Fig. 3.

3.2. Axial force excitation

In a similar manner, the mobility elements relating to an axial force excitation can be rewritten for a numerical analysis. For the axial point force mobility, the normalization with respect to the

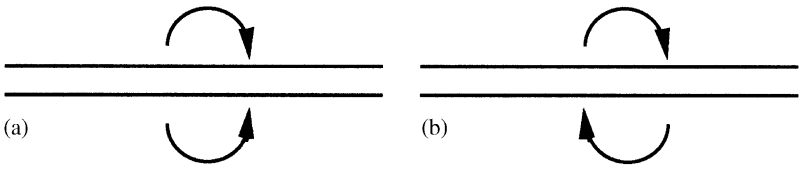

Fig. 3. Symmetric (a) and antisymmetric (b) excitation.

mobility of an infinite rod is appropriate which means that

$$\overline{Y^{\infty}_{v_xF_x}} = \frac{Y^{\infty}_{v_xF_x}}{(1/2Ht\sqrt{E\rho})} = \frac{\mathrm{i}\sqrt{2(1+\nu)}}{\pi}\frac{H}{l}(k_T l) \times \int_0^{\infty} \sqrt{1-\kappa^2}E_F(\kappa)\left(\frac{\tan\left(k_T h\sqrt{\frac{(1-\nu)}{2}-\kappa^2}\right)\tan(k_T h\sqrt{1-\kappa^2})}{\overline{N_1}} - \frac{\cot\left(k_T h\sqrt{\frac{(1-\nu)}{2}-\kappa^2}\right)\cot(k_T h\sqrt{1-\kappa^2})}{\overline{N_2}}\right)\mathrm{d}\kappa, \tag{30}$$

where

$$E_F(\kappa) = \begin{cases} \left(\dfrac{\sin \kappa k_T l}{\kappa k_T l}\right)^2, & \text{soft indenter,} \\ \mathrm{J}_0(\kappa k_T l)^2, & \text{rigid indenter} \end{cases} \tag{31}$$

and $\overline{N_1}$, $\overline{N_2}$ given by Eq. (24). As for moment excitation, the numerical integration is subdivided in three regions. For large M, the integral can, analogous to that of the previous case, be approximated by

$$I_{v_xF_x} \to \frac{2}{(1+\nu)}\int_M^{\infty}\frac{E_F(\kappa)}{\kappa}\mathrm{d}\kappa. \tag{32}$$

The point-cross mobility from an axial force to a lateral rotational velocity normalized with respect to the moment mobility of an Euler beam multiplied by half its depth, take

the form

$$\overline{Y^{\infty}_{w_z F_x}} = \frac{Y^{\infty}_{w_z F_x}}{(\omega H/8Bk_B)} = \frac{4i}{\pi}\left(\frac{(1+\nu)}{6}\right)^{3/4}\left(\frac{H}{l}\right)^{3/2}(k_T l)^{3/2} \times \int_0^{\infty} \kappa^2 \bar{E}_F(\kappa)\left(\frac{(2\kappa^2-1)\tan\left(k_T h\sqrt{\frac{(1-\nu)}{2}-\kappa^2}\right)+2\sqrt{\frac{(1-\nu)}{2}-\kappa^2}\sqrt{1-\kappa^2}\tan\left(k_T h\sqrt{1-\kappa^2}\right)}{\overline{N_1}}\right.$$
$$\left.+\frac{(2\kappa^2-1)\cot\left(k_T h\sqrt{\frac{(1-\nu)}{2}-\kappa^2}\right)+2\sqrt{\frac{(1-\nu)}{2}-\kappa^2}\sqrt{1-\kappa^2}\cot\left(k_T h\sqrt{1-\kappa^2}\right)}{\overline{N_2}}\right)\mathrm{d}\kappa \tag{33}$$

with

$$\bar{E}_F(k) = \begin{cases} \left[\dfrac{\sin \kappa k_T l}{\kappa k_T l}\right]^2, & \text{soft indenter,} \\ \mathrm{J}_0(\kappa k_T l)\dfrac{\sin \kappa k_T l}{\kappa k_T l}, & \text{rigid indenter.} \end{cases} \tag{34}$$

For the third region it is again necessary to carry out the integration in two steps of which the second addresses the tail-integral asymptotically as

$$\mathrm{III}_{tail} I_{w_z F_x} = -2\left(\frac{1-\nu}{1+\nu}\right)\int_M^{\infty} \bar{E}_F(\kappa)\,\mathrm{d}\kappa. \tag{35}$$

The lower limit of integration M is, as before, given by the condition in Eq. (29).

4. Numerical results and discussion

The normalized, axial point mobilities for the two ideal indenters are shown in Figs. 4 and 5. The normalization introduced refers to the (characteristic) mobility of an infinite rod. Owing to the fact that the imaginary part changes its overall character from being stiffness controlled for small Helmholtz numbers to being mass controlled for large, the presentation of this part is split into two diagrams. In the figures, the parameter is the ratio of beam depth to indenter length.

For Helmholtz numbers below the dilatational resonance, the axial point mobility can be interpreted as that of a rod subject to a combined force and moment excitation, reduced to the neutral layer. Owing to the averaging over the excitation area, it is seen that the larger the indenter, the smaller the imaginary part where then the latter essentially stems from the rotational motion. Also indicated is the increased influence of the shear-tensional near field as the ratio of beam depth to indenter length grows large. At high Helmholtz numbers, the features of a waveguide are clearly displayed with an overall diminishing imaginary part. This behaviour can be

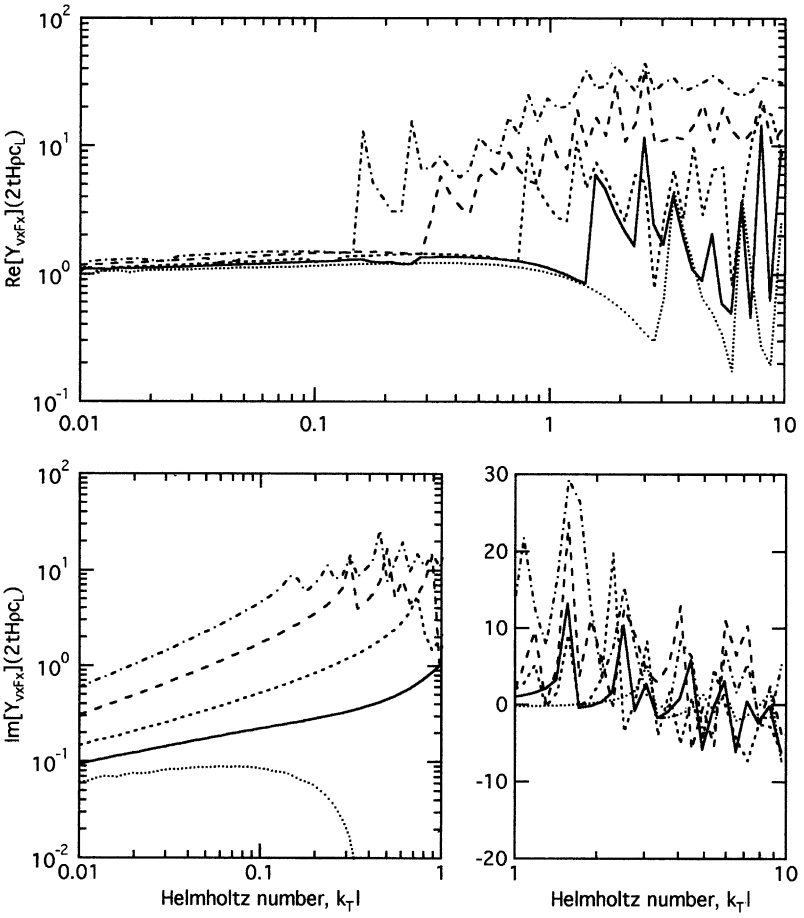

Fig. 4. Normalized real and imaginary parts of axial point force mobility; soft indenter. (· · · ·) $H/2l = 0.5$, (—) $H/2l = 1$, (- - -) $H/2l = 2$, (— —) $H/2l = 5$, (— · —) $H/2l = 10$.

neatly interpreted by employing a fluid acoustic analogy. For a baffled piston, the directivity is enhanced with increasing Helmholtz number (ka where a is the radius of the piston). This means that less and less of the medium outside a hypothetical cylinder of the same cross-sectional dimension as that of the piston participates in the power transmission to the far field. Transferring this reasoning to the structural acoustic case, the real part of the mobility tends to that of a shear stress excited strip, across the depth of the beam, with a width equal to the length of the indenter. By the same token, the imaginary part approaches zero, inversely proportional to Helmholtz number.

In the region of rod behaviour, i.e., for $k_T l < \pi l/h$, the numerical results demonstrate clearly that the rigidity of the indenter is of negligible influence whereas differences can be observed in the waveguide region.

In Figs. 6 and 7, the normalized moment to translational velocity cross-transfer mobility is presented for the two idealized indenters, respectively. The normalization introduced in this case

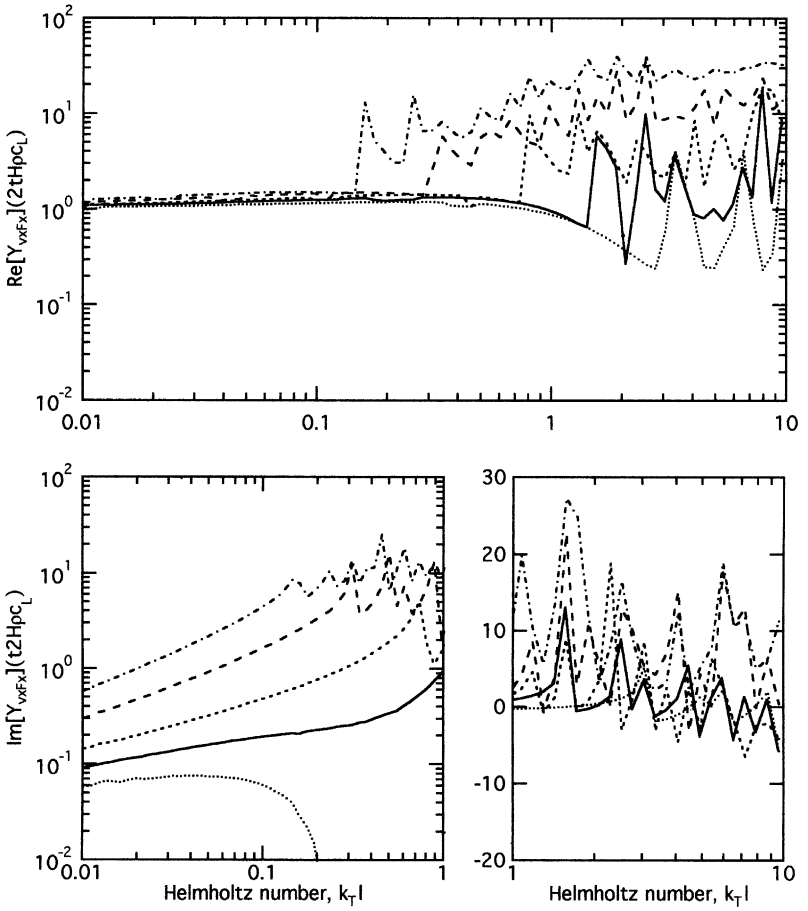

Fig. 5. Normalized real and imaginary parts of axial point force mobility; rigid indenter. (· · · ·) $H/2l = 0.5$, (—) $H/2l = 1$, (- - -) $H/2l = 2$, (— —) $H/2l = 5$, (— · —) $H/2l = 10$.

compares the mobility as calculated employing continuum theory with that obtained due to a pure rotation of the beam lamina, multiplied by the distance from the neutral layer to the excited edge at the response position. In the graphs, the parameter is the ratio of beam height to indenter length, as before. It should be observed that both ordinates, real and imaginary, are negative meaning that a positive moment yields a velocity in the negative x direction, see Fig. 1.

Although not identical, one can see that the rigidity of the indenter is of subordinate influence also for the point-cross mobility from a moment to the axial velocity. Thus, the two sets of curves are practically similar and the discrepancies are mainly noticeable for large Helmholtz numbers, typically $k_T l > 1$. For small Helmholtz numbers and small beam heights, the mobility appears to follow elementary beam theory. The results presented for the imaginary part, however, suggest that the (spatial) averaging of the response over the indenter length reduces this part of the mobility compared with prediction based on elementary theory when the indenter is longer than or equal to the height of the beam. It is also observed that the beam lamina rotation interpretation

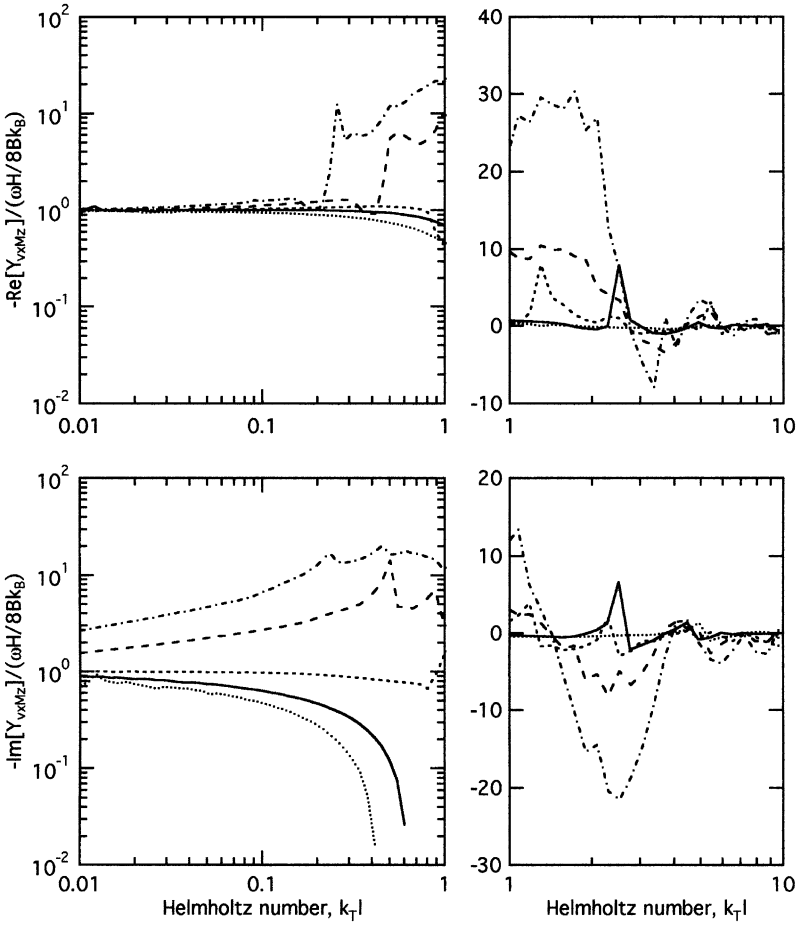

Fig. 6. Normalized real and imaginary parts of moment to translational velocity point-cross mobility; soft indenter. $(\cdots)$ $H/2l = 0.5$, (—) $H/2l = 1$, (- - -) $H/2l = 2$, (——) $H/2l = 5$, (—·—) $H/2\,l = 10$.

is applicable only for very small Helmholtz numbers, $k_T l < 0.1$. At high Helmholtz numbers, the beam constitutes a waveguide with a distinct cut-on at which the beam depth equals half a wavelength for the quasi-longitudinal wave. In the waveguide region, the point-cross mobility is essentially governed by the on-set of higher order in-plane waves. One can note that as the ratio of beam height to indenter length increases, the imaginary part deviates from that given by elementary beam theory, which suggests an enhanced influence of the shear-tensional near field.

'Reciprocity' is addressed by considering the point-cross mobility from axial force to rotational velocity is displayed for the two principal indenters in Figs. 8 and 9. The parameter in the graphs is the same as that in previous diagrams. Again, it is established that the indenter rigidity is of subordinate influence and that elementary beam theory can be employed for the point-cross mobility for small Helmholtz numbers and beam depths. In the graph presenting the soft indenter, imaginary part for small Helmholtz numbers is also included the asymptotic behaviour resulting from a shear-tensional near field as given by Eq. (27). It can be observed that this asymptote

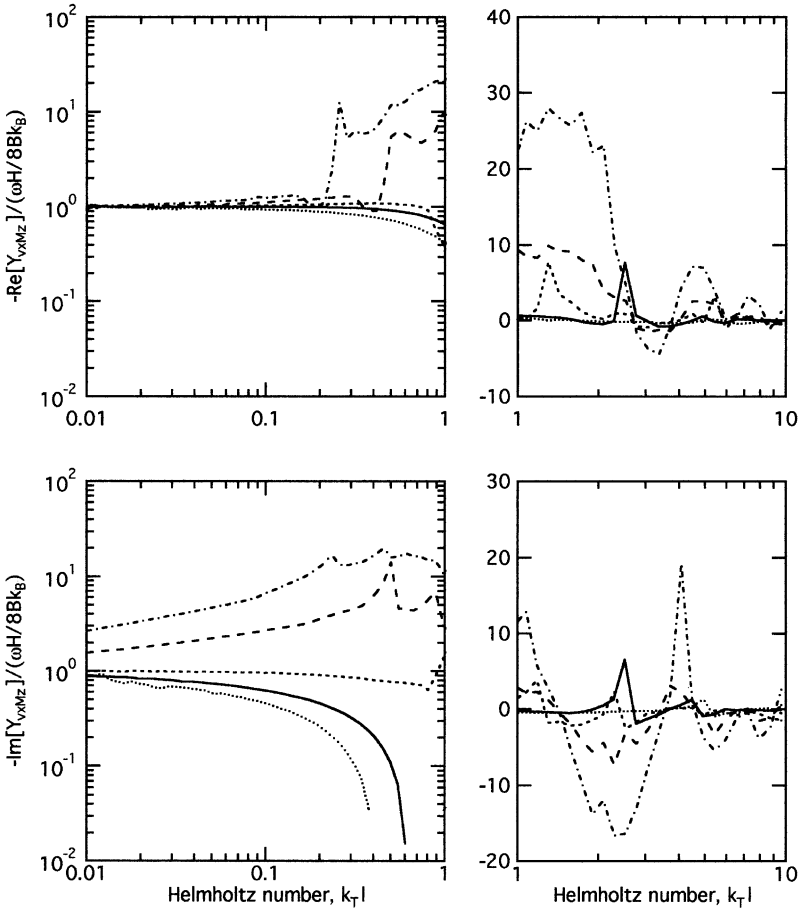

Fig. 7. Normalized real and imaginary parts of moment to translational velocity point-cross mobility; rigid indenter. ($\cdots$) $H/2l = 0.5$, (—) $H/2l = 1$, (- - -) $H/2l = 2$, (— —) $H/2l = 5$, (— · —) $H/2l = 10$.

slightly overestimates the imaginary part, a finding that is ascribed to the fact that the asymptotic behaviour assumes an infinitely deep beam.

In the range immediately above the dilatational resonance, the real parts exhibit a local, more or less broad, maximum for large beam depth to indenter length ratios. It is observed, moreover, that the larger this ratio, the more prominent the waveguide resonances, even though the envelopes slowly decay for high Helmholtz numbers. A similar pattern is found also for the imaginary part.

Upon comparing the point-cross mobilities in Figs. 6 and 8 as well as Figs. 7 and 9 it is evident that the pairs closely resemble those of reciprocal ones for small Helmholtz numbers, $k_T l < 1$. From the upper region, however, it is clear that this is not the case and the theoretically based conclusion of non-reciprocity is numerically corroborated. In practice, the difference may not be important owing to the fact that the wavefield is blurred by resonances for finite structures and wave conversion associated with the presence of discontinuities. Accordingly, reciprocity should

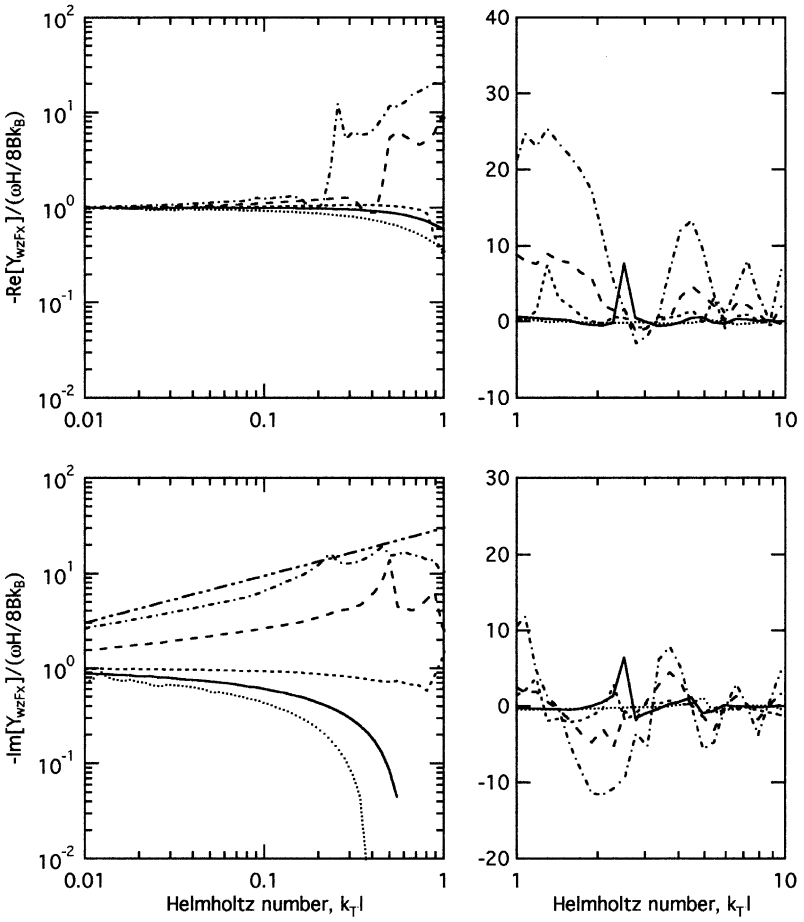

Fig. 8. Normalized real and imaginary parts of axial force to rotational velocity point-cross mobility; soft indenter. (· · · ·) $H/2l = 0.5$, (—) $H/2l = 1$, (- - -) $H/2l = 2$, (— —) $H/2l = 5$, (— —) $H/2l = 10$. (— · —) shear-tensional nearfield for $H/2l = 10$.

be valid in an approximate, overall sense. The basic complication remains, however, that in order to obtain a complete and correct description of the waveguide features, the mobility must be numerically evaluated.

Based on the theoretical and numerical results, an estimation procedure for the axial point mobility can be attempted. For the real part, the procedure simply consists of the characteristic mobility of the associated rod up to $k_T H = 1$ where above is employed the characteristic mobility of the strip of dimensions equal to the indenter length, width and depth of the beam, carrying pure shear waves, as discussed above. When the dilatational resonance occurs below the Helmholtz number of the fully developed shear strip waveguide, i.e., below $k_T l > \pi/2$, the apparent strip width varies in accordance with the piston analogy such that the real part grows with Helmholtz number. This means that the procedure for the real part generally encompasses three ranges. For the imaginary part on the other hand, there is a trade-off between the response due to the (rigid)

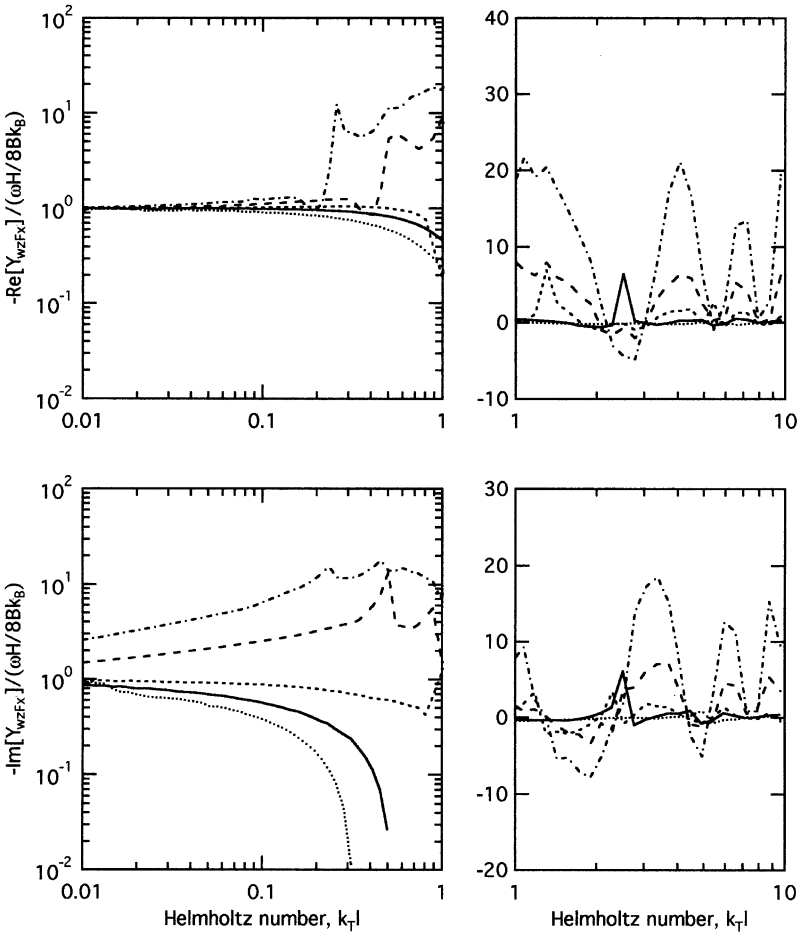

Fig. 9. Normalized real and imaginary parts of axial force to rotational velocity point-cross mobility; rigid indenter. (· · · ·) $H/2l = 0.5$, (—) $H/2l = 1$, (- - -) $H/2l = 2$, (— —) $H/2l = 5$, (— · —) $H/2l = 10$.

beam lamina rotation and that of the shear-tensional near field at Helmholtz numbers below unity whereas a vanishing imaginary part can be assumed there above. As established in the theoretical development, an asymptotic description of the shear-tensional near field is not explicitly available in the case of axial force excitation. From a dimensional analysis, however, based on such descriptions for plates [1] and that derived herein for the point-cross mobility, an approximation can be tentatively devised as

$$\mathrm{Im}[Y_{vF}^{C\infty}] \approx \frac{\omega\pi}{4Gt}. \tag{36}$$

In the region of rod behaviour, this local reaction is then superimposed on the projected beam lamina rotation. For the upper region, the fundamental dependence is taken from the baffled piston analogy. The estimation procedure is compiled in Table 1.

Table 1
Estimation procedure for axial point force mobility

Region	$k_T H \leqslant \pi$ and $k_T l \leqslant \pi/2$	$k_T H \geqslant \pi$ and $k_T l \leqslant \pi/2$	$k_T H \geqslant \pi$ and $k_T l \geqslant \pi/2$
$\mathrm{Re}[Y_{v_x F_x}]$	$\dfrac{1}{2tH\rho c_L}$	$\dfrac{1}{2tH\rho c_L}\dfrac{2}{\pi}k_T l$	$\dfrac{1}{2tH\rho c_T}$
$\mathrm{Im}[Y_{v_x F_x}]$	$\dfrac{\omega H^2}{16Bk_B}+\dfrac{\omega\pi}{4Gt}$	$\dfrac{\pi}{4}\dfrac{\sqrt{\pi k_T H}}{2\rho c_T tH}$	$\dfrac{\pi^3}{4}\dfrac{1}{2\rho c_T tH}\sqrt{\dfrac{H}{2l}}\dfrac{1}{k_T l}$

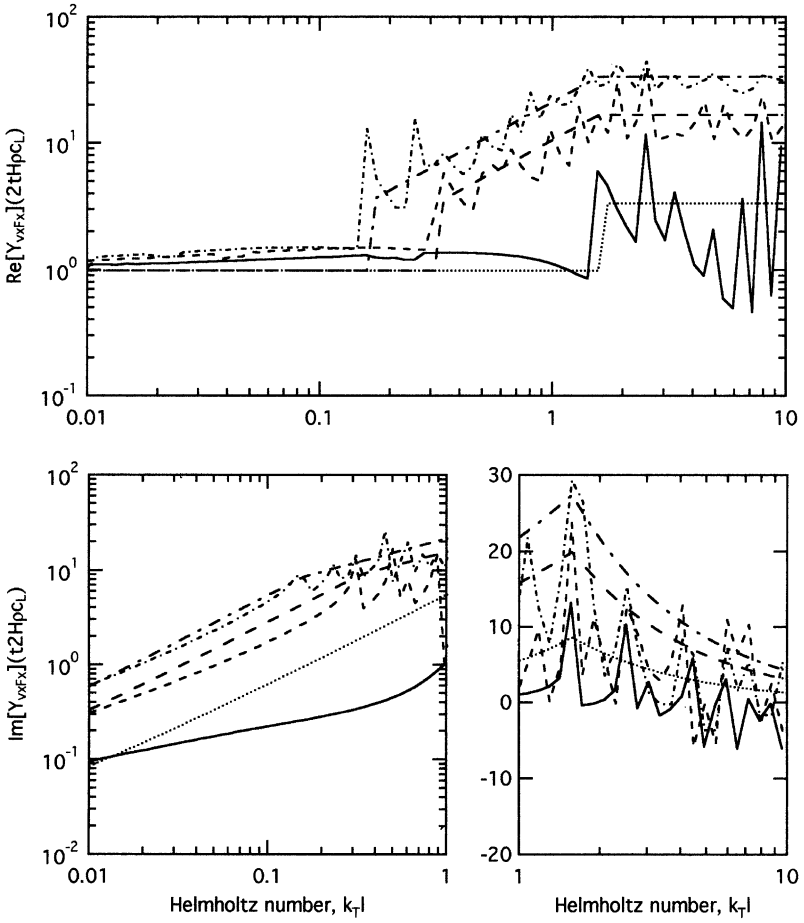

Fig. 10. Comparison of computed and estimated axial point force mobility. $H/2l = 1$ (—) computed and (· · · ·) estimated, $H/2l = 5$ (- - -) computed and (— —) estimated, $H/2\,l = 10$ (- · - · -) computed and (— · —) estimated.

Upon applying this estimation procedure, one obtains a prediction as illustrated in Fig. 10. The comparison clearly demonstrates that the estimation procedure reveals the basic features with respect to the real part, whereas it is inadequate with respect to the imaginary for small ratios of the beam height to indenter length. Accordingly there is an additional ingredient, which might be

linked to the increased influence of shear, and thereby an additional dependence on the indenter size, not revealed by the dimensional analysis employed.

Regarding the point-cross mobilities, the numerical results suggest that a cross-sectionally integrated beam theory is applicable for small Helmholtz numbers and limited beam depths, irrespective of the indenter rigidity. This means that the cross-coupling between either a moment and the axial velocity or an axial force and the rotational velocity can be simply viewed as the axial velocity at the edge of a rotating rigid beam lamina resulting from the moment applied in the former case and as the rotational velocity of the beam lamina due to the equivalent moment resulting from the axial force times the lever of half the beam depth. Tentatively, one may set the upper limit of applicability for approximations based on such reasoning to $k_T l < \pi l/H$ or equivalently $k_T H < \pi$. As the beam becomes deep in comparison with the length of the indenter, the shear-tensional nearfield affects the response and the imaginary part as obtained from elementary beam theory must be augmented by the contribution from the nearfield. Accordingly, an approximation for the point-cross mobility can be proposed on the form

$$Y_{v_x M_z} \approx -\frac{\omega H}{8Bk_B}\left\{1 + \mathrm{i}\left[1 + \frac{(1-\nu)}{3}\left(\frac{H}{l}\right)^2 k_B l\right]\right\}, \tag{37}$$

whereby it is seen that the shear-tensional nearfield only comes into play for

$$k_B l > \frac{3}{(1-\nu)}\left(\frac{l}{H}\right)^2. \tag{38}$$

Thus, an estimation procedure for these mobility elements in the region of small Helmholtz numbers can be compiled as in Table 2.

In Fig. 11 are compared the estimated and computed results for three ratios of beam depth to indenter length. For the point-cross mobilities as well, the estimation procedure yields reasonable real parts up to the dilatational resonance. With the normalization introduced all curves coincide and are unity. In contrast, too large imaginary parts which indicates that the reactive behaviour has a more intricate dependence on the beam height to indenter length ratio than revealed by the asymptotic analysis. It is seen, however, that the slope is correctly captured for depth to length ratios equal to five or larger. It should be noted that spatial averaging is not considered in the estimation procedure, which enhances the discrepancies for slender beams and large indenters.

Table 2
Estimation procedure for point-cross mobilities

Region	$k_T l \leqslant \pi l/H$	$k_T l > \pi l/H$
$\mathrm{Re}[Y_{w_z F_x}] \approx \mathrm{Re}[Y_{v_z M_x}]$	$-\dfrac{\omega H}{8Bk_B}$	—
$\mathrm{Im}[Y_{w_z F_x}] \approx \mathrm{Im}[Y_{v_z M_x}]$	$-\dfrac{\omega H}{8Bk_B}\left[1 + \dfrac{(1-\nu)}{3}\left(\dfrac{H}{l}\right)^2 k_B l\right]$	—

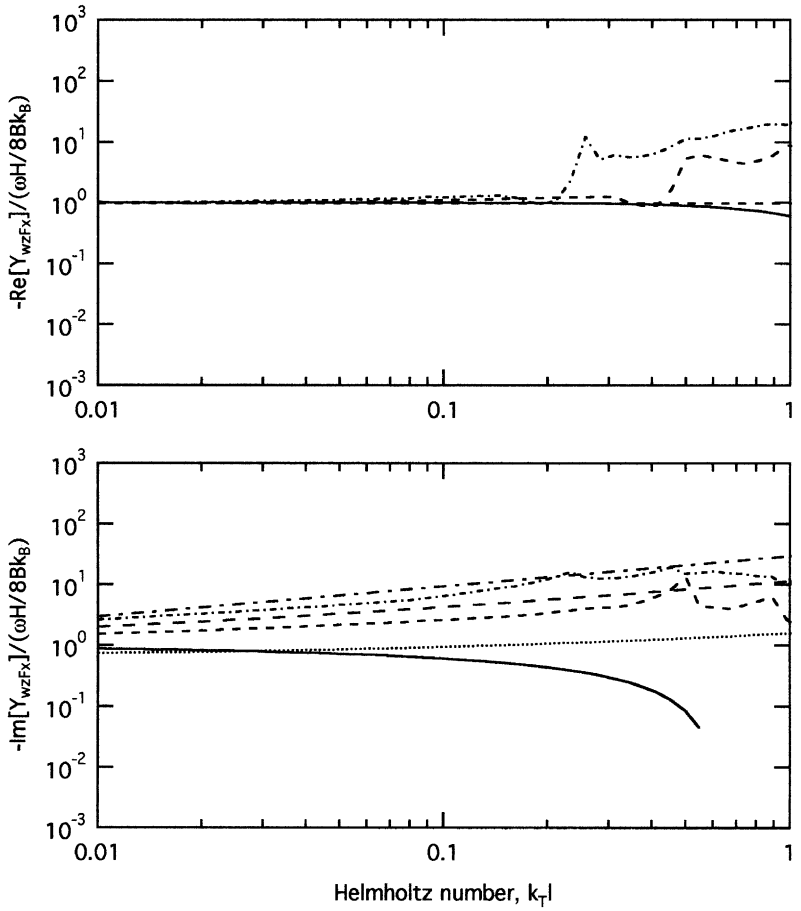

Fig. 11. Comparison of computed and estimated point-cross mobility. $H/2l = 1$ (——) computed and (· · · · · ·) estimated, $H/2l = 5$ (- - -) computed and (— —) estimated, $H/2l = 10$ (- · - · -) computed and (— · —) estimated.

Approximations for the upper region have not been pursued since the waveguide effects controlling the cross-coupling between the orthogonal excitation and response components depend on the actual stress distribution.

5. Concluding remarks

The multi-point and multi-component transmission requires knowledge of point-cross and cross-transfer mobilities beside the point and transfer mobility elements for the general case. The former elements are of particular interest for configurations where the contact areas are displaced from the neutral layer of a receiver in bending so that excitation and response components may also be geometrically coupled.

The three primary questions raised, are the point-cross mobilities reciprocal, are cross-sectionally integrated theories applicable, and is there an influence of the shear-tensional near

field, have been addressed and it can be concluded that the shear-tensional near field does indeed influence the point-cross mobilities for small indenters and deep beams. Likewise, though anticipated, the axial point force mobility is affected under the same conditions but an explicit expression has not been established. The contribution to the imaginary part from the shear-tensional near field, moreover, is found dominant for ratios of beam depth to indenter length greater than five, which implies that the imaginary part is not adequately described solely by this field for slender or moderately deep beams but the continuum theoretical expression must be employed.

The two point-cross mobilities have been demonstrated to be strictly reciprocal solely in the hypothetical case of point excitation. The deviation from a reciprocal state, however, is practically negligible for realistic excitation conditions in the range below the dilatational resonance. For large Helmholtz numbers, discrepancies are noticeable but reciprocity can still be applied in an approximate, overall sense when the prediction of the waveguide effects are of subordinate importance.

For both kinds of cross mobility elements, the inter-relation between ordinary bending, shear and the shear-tensional near field is quantitatively complicated and only for the extreme configurations, slender and very deep beams, respectively, typical deformations can be identified. This means that cross-sectionally integrated theories such as Euler–Bernoulli or Timoshenko are inadequate. In turn, the rigid beam lamina rotation model is only applicable as a basis for developing the point-cross mobility elements for very small Helmholtz numbers, $k_T l$, (strictly as Helmholtz number approaches zero) and a correct imaginary part must be computed from continuum theory.

The effects of the shear-tensional near field in the case of axial point force excitation can be cautiously extrapolated from the point moment mobility [1] and the point-cross mobility from moment to axial velocity derived in this work where closed form, asymptotic expressions have been obtained. With such a procedure, however, it should be borne in mind that the expressions resulting do not reveal the influence of variations in the excitation stress field.

For practically realistic dimensions of beams in vehicles, buildings and ships, it is clear that the cross mobilities will be influential and cannot be omitted a priori in an analysis. In particular, it is found, that the range around the dilatational resonance can be significant. This is so for two reasons. First, the real part is a maximum and second, the imaginary part is negative and partially controlled by the size of the indenter implying that matching in dynamic characteristics can occur for out of phase, complementary excitation components.

For the point-cross mobilities, taken to be reciprocal in an overall sense, as well as the axial point force mobility, estimation procedures have been attempted which satisfactorily depict the trends of the real parts. With respect to the imaginary parts, only the extreme cases of slender or very deep beams are acceptably predicted. This deficiency can be primarily referred to the increased influence of shear as the beam height to indenter size ratio increases and as the wavelength decreases. Accordingly, the employment of Timoshenko theory should markedly improve the estimation procedures for intermediate cases.

Acknowledgements

The financial support received from TNO Institute of Applied Physics is gratefully acknowledged.

Appendix A. Coefficient matrix

The divergence free and irrotational fields can be described in terms of the stream and vector potential functions. For the present, two-dimensional problem, the vector character of the potential function is unnecessary and a scalar version is sufficient

$$\Phi(x,y) = \{\Phi_1 \cos(q_L y) + \Phi_2 \sin(q_L y)\} e^{ikx}, \tag{A.1}$$

$$\Psi(x,y) = \{\Psi_1 \cos(q_L y) + \Psi_2 \sin(q_L y)\} e^{ikx}. \tag{A.2}$$

The axial and transverse velocity components can be obtained from the relations

$$v_x = \Phi_{,x} + \Psi_{,y}, \quad v_y = \Phi_{,y} + \Psi_{,x}, \tag{A.3a, b}$$

where a comma means differentiation with respect to the co-ordinates following.

For a linearly elastic material in a state of plane stress, the constitutive equations can be written as

$$\sigma_x = \frac{2G}{i\omega(1-\nu)}(\Phi_{,xx} + \Psi_{,xy} + \nu(\Phi_{,yy} + \Psi_{,xy})), \tag{A.4a}$$

$$\sigma_y = \frac{2G}{i\omega(1-\nu)}(\Phi_{,yy} + \Psi_{,xy} + \nu(\Phi_{,xx} + \Psi_{,xy})), \tag{A.4b}$$

$$\tau_{xy} = \frac{2G}{i\omega}\left(\Phi_{,xy} + \tfrac{1}{2}(\Psi_{,yy} - \Psi_{,xx})\right). \tag{A.4c}$$

This means that for the upper edge where $y = h$

$$\begin{aligned} 0 = {} & (q_L^2 + \nu k^2)\{\Phi_1 \cos(q_L h) + \Phi_2 \sin(q_L h)\} \\ & - (1-\nu) ikq_T \{\Psi_1 \sin(q_T h) - \Psi_2 \cos(q_T h)\} \end{aligned}$$

and

$$\begin{aligned} \frac{i\omega}{2G}\hat{\tau} = {} & ikq_L\{-\Phi_1 \sin(q_L h) + \Phi_2 \cos(q_L h)\} \\ & + \frac{k^2 - q_T^2}{2}\{\Psi_1 \cos(q_T h) + \Psi_2 \sin(q_T h)\}, \end{aligned}$$

whereas at the lower, i.e., $y = -h$

$$\begin{aligned} 0 = {} & (q_L^2 + \nu k^2)\{\Phi_1 \cos(q_L h) - \Phi_2 \sin(q_L h)\} \\ & + (1-\nu) ikq_T \{\Psi_1 \sin(q_T h) + \Psi_2 \cos(q_T h)\} \end{aligned}$$

as well as

$$\begin{aligned} 0 = {} & ikq_L\{\Phi_1 \sin(q_L h) + \Phi_2 \cos(q_L h)\} \\ & + \frac{k^2 - q_T^2}{2}\{\Psi_1 \cos(q_T h) - \Psi_2 \sin(q_T h)\}. \end{aligned}$$

The coefficients C_{kn} can now be identified to be

$$C_{11} = (q_L^2 + vk^2)c_L, \quad C_{12} = (q_L^2 + vk^2)s_L, \quad C_{13} = -(1-v)\mathrm{i}kq_T s_T, \quad C_{14} = (1-v)\mathrm{i}kq_T c_T,$$

$$C_{21} = (q_L^2 + vk^2)c_L, \quad C_{22} = -(q_L^2 + vk^2)s_L, \quad C_{23} = (1-v)\mathrm{i}kq_T s_T, \quad C_{24} = (1-v)\mathrm{i}kq_T c_T,$$

$$C_{31} = -\mathrm{i}kq_L s_L, \quad C_{32} = \mathrm{i}kq_L c_T, \quad C_{33} = \frac{(k^2 - q_T^2)}{2} c_T, \quad C_{34} = \frac{(k^2 - q_T^2)}{2} s_T,$$

$$C_{41} = \mathrm{i}kq_L s_L, \quad C_{42} = \mathrm{i}kq_L c_L, \quad C_{43} = \frac{(k^2 - q_T^2)}{2} c_T, \quad C_{44} = -\frac{(k^2 - q_T^2)}{2} s_T,$$

wherein the abbreviations $c_L = \cos(q_L h)$, $s_L = \sin(q_L h)$, $c_T = \cos(q_T h)$ and $s_T = \sin(q_T h)$ have been used.

Thus, the matrix $\mathbf{C}$ can be established as

$$\mathbf{C} = \begin{bmatrix} C_{11} & C_{12} & C_{13} & C_{14} \\ C_{11} & -C_{12} & -C_{13} & C_{14} \\ C_{31} & C_{32} & C_{33} & C_{34} \\ -C_{31} & C_{32} & C_{33} & -C_{34} \end{bmatrix} \tag{A.5}$$

and the determinant is readily obtained as

$$\mathrm{Det}[C] = 4\{(C_{11}C_{34} - C_{14}C_{31})(C_{12}C_{33} - C_{13}C_{32})\}. \tag{A.6}$$

With $\mathbf{D} = \mathbf{C}^{-1}$, the elements required in view of the axial excitation are

$$D_{13} = \frac{Cof(C_{31})}{\mathrm{Det}[C]}, \quad D_{23} = \frac{Cof(C_{32})}{\mathrm{Det}[C]}, \quad D_{33} = \frac{Cof(C_{33})}{\mathrm{Det}[C]}, \quad D_{34} = \frac{Cof(C_{34})}{\mathrm{Det}[C]}. \tag{A.7a, b, c, d}$$

From (A.5) the co-factors can be developed as

$$Cof(C_{31}) = -2C_{14}(C_{12}C_{33} - C_{13}C_{32}), \tag{A.8a}$$

$$Cof(C_{32}) = -2C_{13}(C_{11}C_{34} - C_{14}C_{31}), \tag{A.8b}$$

$$Cof(C_{33}) = -2C_{12}(C_{11}C_{34} - C_{14}C_{31}) \tag{A.8c}$$

and

$$Cof(C_{34}) = -2C_{11}(C_{12}C_{33} - C_{13}C_{32}). \tag{A.8d}$$

Upon substituting Eqs. (A.6) and (A.8) into Eqs. (A.7), using the elements of $\mathbf{C}$ established above, the stream and potential functions in Eqs. (13) result.

Appendix B. Nomenclature

B flexural stiffness
$\mathbf{C}$ coefficient matrix
$\mathbf{D}$ coefficient matrix
E excitation spectrum, Young's modulus

F force
G shear modulus
H beam height
I integral
J Bessel function
M moment
N denominator
S surface
Y mobility
h half the beam height
i imaginary unit
k wavenumber
l half the indenter length
q wavenumber radical
t beam width
v translational velocity
w rotational velocity
x, y, z Cartesian co-ordinates
Φ, $\mathbf{\Phi}$ Potential function, amplitude vector
Ψ stream function
κ normalized wavenumber
η loss factor
ω angular frequency
ρ density
σ, $\boldsymbol{\sigma}$ normal stress, stress vector
τ shear stress
ν the Poisson ratio

Subscripts
B flexural
F force
L longitudinal
M moment
T transverse
r rigid
s soft
v lateral translational velocity
w lateral rotational velocity
p, q region index
∞ infinite beam

Symbol
$\bar{\ }$ spatially averaged

References

[1] B.A.T. Petersson, M. Heckl, Concentrated excitation of structures, Journal of Sound and Vibration 196 (1996) 295–321.
[2] R.D. Mindlin, Influence of rotatory inertia and shear on flexural motions of isotropic, elastic plates, Journal of Applied Mechanics 18 (1951) 31–38.
[3] S.P. Timoshenko, D.H. Young, W. Weaver Jr., Vibration Problems in Engineering, 4th Edition, Wiley, New York, 1974.
[4] B.A.T. Petersson, Concentrated force excitation of deep beams, Journal of Sound and Vibration 224 (1999) 243–266.
[5] M. Heckl, Körperschallübertragung bei homogenen Platten beliebiger Dicke, Acustica 49 (1981) 183–191.
[6] G.N. Bycroft, Forced vibrations of a rigid circular plate on a semi-infinite elastic space and on an elastic stratum, Philosophical Transactions of the Royal Society of London A 248 (1956) 327–368.
[7] S. Ljunggren, Generation of waves in an elastic plate by a vertical force and by a moment in the vertical plane, Journal of Sound and Vibration 90 (1983) 559–584.
[8] S. Ljunggren, Generation of waves in an elastic plate by a torsional moment and by a horizontal force, Journal of Sound and Vibration 93 (1983) 161–187.
[9] R.C.N. Leung, Vibration transmission from deck to hull via a bulkhead, Journal of Sound and Vibration 213 (1998) 551–560.
[10] B.A.T. Petersson, A thin-plate model for the moment mobility at T-intersections of plates, Journal of Sound and Vibration 108 (1986) 471–485.